Engineered Science
DOI: https://dx.doi.org/10.30919/es1037

The Effect of Plasmons of Silver Nanoparticles on the Luminescence of S,N-doped Carbon Dots

Niyazbek Ibrayev,[1,*] Aygul Nuraje,[2] Gulnur Amanzholova,[1] Evgeniya Seliverstova[1,*] and Takhmina Khamza[3]

Abstract

The plasmon effect of Ag nanoparticles on the generation and deactivation of singlet and triplet electron states was studied in solid films of S- and N-doped carbon dots. For this, carbon dots were synthesized with the sizes from 4 to 10 nm. The best emissivity was found for carbon dots based on the citric acid and L-cysteine at the ratio of 1:0.5. It is shown that synthesized carbon dots efficiently generate triplet-excited states. Their deactivation is carried out in two ways – through phosphorescence (at ~560 nm) and delayed fluorescence (at ~440 nm). At the same time, the effect of silver nanoparticles on the absorption and luminescence of carbon dot films was studied. It has been demonstrated for the first time that the presence of Ag nanoparticles leads to the growth in the intensity of long-lived luminescence of carbon dots. The intensity of fluorescence was increased by 1.6 times, and long-lived luminescence – by 2.7 times. The effect of the luminescence enhancement of carbon dots can be in demand in such applications as photodynamic therapy, bioimaging, anti-counterfeiting coatings and latent imaging, organic light-emitting diods, sensors, *etc*.

Keywords: Carbon dots; Citric acid; L-cysteine; Luminescence ; Plasmon effect.
Received: 08 November 2023; Revised: 21 November 2023; Accepted: 30 November 2023.
Article type: Research article.

1. Introduction

Carbon dots (CDs) are quasi-spherical or spherical particles with a diameter of less than 10 nm. They are representing a core/shell structure consisting of a carbon core with graphite fragments and a shell from various surface functional groups.[1,2] CDs have attracted close attention due to their unique properties and some advantages over organic molecules and traditional semiconductor quantum dots. CDs, along with high chemical resistance and photostability, have a high emission efficiency, good biocompatibility, and low toxicity.

The photoluminescence of CDs are originated from the chemical groups of atoms included in the conjugated bonds of the core and/or surface chromophore groups.[2] The unquestionable advantage of CDs is that, along with fluorescence, they also have an afterglow. The afterglow, as a rule, is red-shifted relative to the fluorescence of CDs that expands the possibilities of their practical usage. In addition, the afterglow indicates the formation of triplet-excited CDs. This effect can be used to generate singlet oxygen and for biomedical applications,[3,4] as well as in optoelectronic and photocatalytic devices.[5,6]

Moreover, it was shown that by means of directed synthesis it is possible to control not only the position of CDs fluorescence and long-lived luminescence on the wavelength scale, but also its efficiency.[2,7] The dependence of the luminescent properties of CDs on the synthesis conditions is a very popular scientific problem due to the advantages of CDs over organic fluorophores and semiconductor quantum dots. CDs possess chemical stability and photostability, high luminescence efficiency, good biocompatibility and low toxicity. This determines their application in various fields, such as in bioimaging,[2] protective coatings,[8] light emitting diodes (LEDs), solar cells,[9] lasers, sensors and molecular electronics.[10,11]

However, CDs synthesized on the basis of citric acid only, or urea, or L-cysteine, have a number of disadvantages, such as a low fluorescence quantum yield (no more than 10%),[2,7] the using of ultraviolet (UV) light for their photoexcitation and luminescence of such CDs in the predominantly blue region of the spectrum that significantly limits their practical use. The low values of the fluorescence quantum yield of such CDs are the result of strong carbonization of the carbon core and a

[1] *Institute of Molecular Nanophotonics, Buketov Karaganda University, Karaganda 100024, Kazakhstan.*
[2] *Brooklyn Technical High School, Brooklyn, New York 11217, USA.*
[3] *Istanbul Technical University, Istanbul 34485, Turkey.*
**Email:* niazibrayev@mail.ru (N. Ibrayev); genia_sv@mail.ru (E. Seliverstova)

small number of surface functional groups and conjugated structures. Meanwhile, the presence of surface states and their conjugation with the carbon core are the key factors determining the efficiency of CDs luminescence.[2] To increase the fluorescence quantum yield of CDs up to 80–90%, they can be doped with heteroatoms, such as nitrogen,[11,12] sulfur,[7] silicon,[13] and halogen atoms.[14]

In addition, the luminescent ability of CDs can be enhanced by using the phenomenon of localized plasmon resonance (LPR) of metal nanoparticles (NPs).[15-18] At present, the plasmon effect is actively used to increase the efficiency of photoprocesses in organic molecules, and in semiconductor quantum dots because the rates of photophysical reactions are changed near plasmonic NPs.[19-22]

For CDs, the effect of plasmonic NPs was used only for the enhancement of fast fluorescence.[15-18] In particular, the effect of the plasmon resonance of the Ag NPs on the luminescent properties of CDs with blue, green and yellow emission was studied in Ref. [15] It is shown that it is possible to achieve an increase in the intensity of CDs with green and yellow luminescence when the Ag/SiO_2 core/shell structures with a shell thickness of 15 nm are used. Whereas under the same conditions, Ag NPs extinguishes the blue-luminescent CDs due to the strong overlap of the Ag NPs absorption and CDs fluorescence. The authors of Ref. [16] prepare a series of gold slits, which were used to immobilize CDs in them. The largest increase of fluorescence intensity, equal to ~5.5 times, was obtained at a slit width of 100 nm. In Ref. [17] CDs-gold nanoparticle photonic crystals were obtained. In the synthesized samples a threefold increase in the fluorescence intensity was registered compared to CDs placed simply in a photonic crystal. Authors of Ref. [18] have demonstrated that fivefold enhancement of fluorescence could be achieved by chemically binding CDs to the gold NPs. The observed intensity growth is associated with an ultrafast resonant energy transfer from the gold NPs to the bound CD. Composites based on CDs and plasmonic metal NPs were used to detect mercury ions,[23] chlorophyll,[24] anticancer drugs,[25] *etc*.

In the present work, the effect of plasmonic Ag NPs on the properties of fast and long-lived luminescence of CDs films with various compositions was studied. The composition was varied by changing the ratio of citric acid and L-cysteine. We have not practically found works devoted to the plasmonic enhancement of the CDs afterglow. Also, silver films were used in present work, rather than chemically attached gold NPs or more complex nanostructures, as in Refs. [15-18]. The preparation of our structures does not require careful chemical synthesis and the using of additional reagents that makes the proposed method for obtaining of plasmon-enhanced luminescence of CDs more attractive in practical terms. Meanwhile, the results obtained in this work could be attractive for the development of materials based on CDs and plasmon NPs with better luminescence ability. The effect of enhancement of long-lived luminescence, for the observation of which does not required vacuumization of the sample or low temperatures, makes possible for its practically usage. The afterglow of CDs associated with the deactivation of their triplet-excited states can potentially improve the bioimaging due to the exclusion of noise associated with autofluorescence of biological tissues.[26] But, it is more importantly, enhanced long-lived luminescence of CDs will be in demand for the generation of active forms of molecular oxygen and singlet oxygen. Singlet oxygen is used for the deactivation of cancer cells,[27] antibacterial therapy,[28,29] in the treatment of skin and respiratory diseases[30] and others.

2. Experimental section

The citric acid (CA, content ≥99.5%, catalogue #251275, Sigma Aldrich) was used as a carbon source and L-cysteine (content ≥98%, catalogue #C7352, Sigma Aldrich) was used as a source of N– and S–containing groups.

The synthesis of CDs was performed by microwave synthesis method (Monowave 200, Anton Paar) at 200 °C for 1 hour with intensive stirring according to the procedure detailed in Ref. [7] and shown in the Scheme 1. Microwave synthesis was chosen due to its high speed and reproducibility, as well as the ability to control the temperature and pressure inside the reaction volume. These parameters are of great importance because they have a noticeable effect on the degree

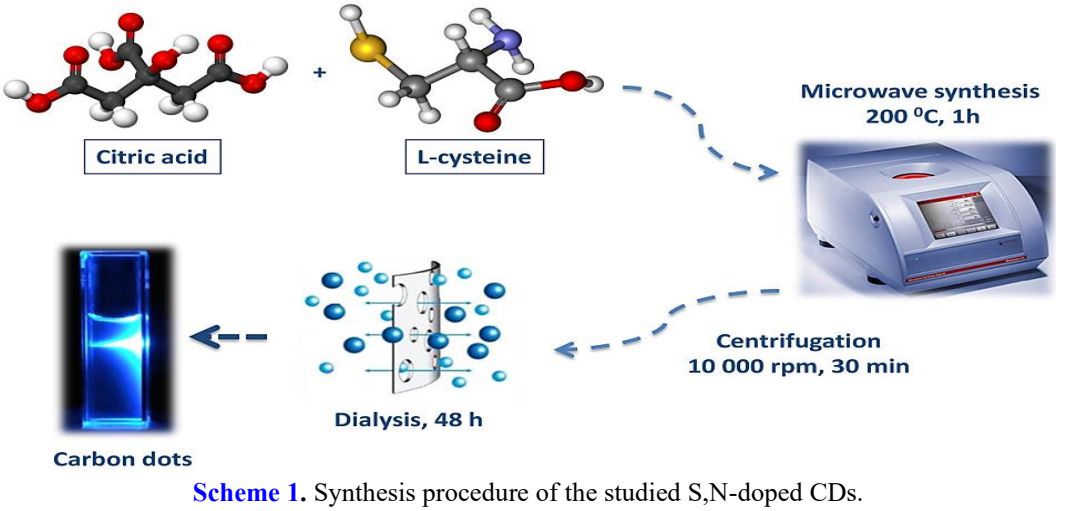

Scheme 1. Synthesis procedure of the studied S,N-doped CDs.

of carbonization of CDs and its optical properties.[1]

To track the CDs composition and their sulfur- and nitrogen doping degree impact their luminescent properties, the CA:L-cysteine ratio was changed. CDs were synthesized with CA:L-cysteine ratios of 1:0 (CDs 1:0, CA-based only), 1:0.5 (CDs 1:0.5), and 1:1 (CDs 1:1). As we showed earlier,[7] an increase in the L-cysteine part in CDs (ratio 1:2) leads to a decrease in the luminescent ability of the samples. When citric acid and amino-containing precursors are used, carbon-containing nanoparticles are formed. Luminescent properties of these particles are attributed to carbon cores in composition with organic fluorophores.

It has been shown that the main structural units and actual sources of fluorescence of S,N-doped CDs are 5-oxo-3,5-dihydro-2H-thiazolo[3,2-a]pyridine-3,7-dicarboxylic acid (TPDCA) and 5-oxo-3,5-dihydro-2H-thiazolo[3,2-a]pyridine-7-carboxylic acid (TPCA) when citric acid and L-cysteine were used.[2,31] An excess of L-cysteine leads to an increase in nonradiative transitions in the surface groups of CDs, which will be expressed in a decreased luminescence quantum yield.[7]

The color of the resulting solution depended on the ratio of CA:L-cysteine and ranged from light yellow (1:0) to dark brown (1:1) (Fig. 1). The synthesized solution was centrifuged at 10000 rpm for 30 minutes. After that, the upper part of the solution was purified by dialysis at 3.5 kDa MWCO.

For the preparation of solid films, CDs solutions with same volumes (500 μL) were dropped onto quartz substrates with a sizes of 15x25 mm and left in an oven at a temperature of 50 ºC until completely dry (24 hours).

To study the effect of plasmon resonance of silver NPs, CDs solutions were deposited over a top of silver island films (SIF) on the same quartz substrates. The island films with a thickness of 5 nm were prepared by magnetron sputtering (Q150R ES, Quorum Technol.) of silver in the half of the substrate with the following annealing of films at 240 ºC for 30 min. During the annealing process, a continuous film breaks and droplet-like islands of silver are formed. In scanning electron microscope (SEM) images (Mira LMU, Tescan), they appear as spherical particles with a radius of 50 – 80 nm (Fig. 1). The space between them was occupied by particles with a smaller radius of 20 – 40 nm. As it was shown by atomic-force microscopy (AFM) measurements (JSPM-5400, Jeol), the thickness of the CDs film on the surface of the substrate and the SIF surface is the same and its thickness is ~ 0.08±0.02 μm (Fig. 1b). The choice of silver for the preparation of plasmonic particles is due to the fact that among metals whose NPs exhibit plasmon properties, silver has good stability and high optical response in the blue region of the spectrum with a maximum of about 400 – 420 nm. Thus, the plasmon resonance band of Ag NPs has a large overlap with the CDs spectra. Since the interaction between NPs and CDs has an electro-dipole character,[19,22,32] the presence of common frequencies in such a system is of a great importance for ensuring the effective interaction of components in it.

The structure and size of CDs were studied using a high-resolution transmission electron microscope (TEM, JEM-2100F/Cs/GIF, Jeol). An accelerating voltage of 200 kV was used to obtain the images. Data on the sizes of synthesized CDs were also obtained by the dynamic light scattering (DLS) method with a Nano 90S analyzer (Malvern). In this case, data obtained from the number-weighted distribution (% number) were used. The standard deviation in determining the CDs diameter was ±1.62 nm. For TEM method, the diameter of the visualized CDs was determined directly from the images with their subsequent averaging. The standard deviation is ±1.5 nm. Fourier-transform infrared (FTIR) spectra were registered on an FSM 1201 spectrometer (Infraspec) in transmission mode. CDs solutions were transferred into an ethanol-water mixture (ratio 10:1 by volume) and applied to the surface of KBr plates, followed by complete drying of the solvent. After this, the transmission spectra of the samples under study were measured, corrected for the influence of the air background, where clean KBr plates acted as reference samples. Also, the CDs structure was studied by X-ray photoelectron microscopy (XPS) method. The XPS spectra were recorded on the Axis Ultra DLD spectrometer (Kratos Analytical) at transmission

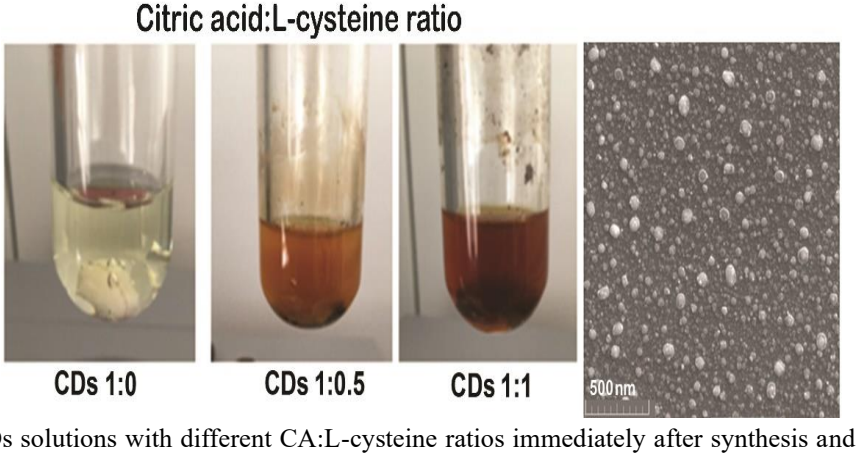

Fig. 1 Photography of CDs solutions with different CA:L-cysteine ratios immediately after synthesis and SEM image of SIF after annealing.

energy of 160 eV (survey) and 40 eV (high-resolution spectra). The registration was carried out with an AlKα source. Calibration was performed according to the C1s component at 285.0 eV.

Absorption spectra were registered with Cary 300 spectrophotometer (Agilent). The spectral width at registration was equal to 2 nm. Emission spectra were measured with an Eclipse spectrometer (Agilent). The bandwidth for the fast fluorescence measurements was 2.5 nm both for the excitation and registration. The measurements were carried out at room temperature and atmospheric pressure. For long-lived luminescence spectra, the bandwidth was chosen to be 10 nm for excitation and recording monochromators. During the measurements of long-lived luminescence spectra, the emission signal was recorded 300 μs after the end of the Xe lamp flash. The decay kinetics of long-lived luminescence was registered with FLS1000 spectrometer (Edinburgh Instr.) with UV/Vis-PMT (Hamamatsu) at a time delay 10 μs after the laser pulse. Photoexcitation of the samples at λ_{exc}=350 nm was carried out by a laser system based on an Nd:YAG laser LQ529, a LP604 parametric light generator and a LG305 second harmonic generator (SolarLS). A vacuum-operated Optistat DN-V cryostat (Oxford Instr.) with the possibility to change the sample temperature from 70 to 500 K was used. A liquid nitrogen as a cooling agent was used.

The fluorescence kinetics was measured on spectrofluorimeter with picosecond resolution and registration in the time-correlated photon counting mode (TCSPC, Becker&Hickl). The samples were excited using a diode laser with λ_{gen}=375 nm, τ=120 ps. Fluorescence lifetimes were estimated with SPC Image software (Becker&Hickl). The intensity of fluorescence decay was described with the equation:[33]

$$I(t) = \sum_{i=1}^{n} \alpha_i \, exp(-t/\tau_i) \quad (1)$$

where τ_i is the lifetime of the excited state (signal decay time), α_i is the amplitude or fraction of the contribution of the i-th component ($\sum_i \alpha_i$ = 1.0). The quality of fitting of the decay curves was estimated from the χ^2 value.

The fluorescence quantum yield (φ_f) of CDs at λ_{exc}=350 nm was estimated according to the method used in Refs. [7,12] Quinine bisulfate with a fluorescence quantum yield of 55% was chosen as a standard.[34]

3. Results and discussion

Previously, we have shown that along with vibrations of carbon and C–H bonds, oxygen-containing (–COO and C=O) groups are presented in the FTIR spectra of CDs based on CA only.[7] CDs obtained with using of L-cysteine (Fig. 2) exhibits O–H stretching vibration band at 3500 cm^{-1}, as well as C–O stretching vibration band at 870 cm^{-1}, which indicate carboxylic acid and other oxygen-containing functional groups.[35] Also in the FTIR spectra, bands around 3050–3250 cm^{-1} appear which related to vibrations of N–H bonds. The intense peak at ~1720 cm^{-1} is the result of stretching vibrations of the C=O bond in α,β-unsaturated carboxylic acid fragments, which is present in citrazine acid and its derivatives,[35] formed during the synthesis of CDs from CA. The peak at ~1620 cm^{-1} is attributed to the stretching vibrations of the C=C bond. It can be noted that the number of oxygen-containing groups in CDs synthesized from CA and L-cysteine increases. The doping of CDs is indicated by the presence of the stretching vibrations of N–H and –SH groups. An increase in the L-cysteine in CDs leads to the intensification of oxygen-, nitrogen-, and sulfur-containing groups. An increase in oxygen-containing groups can induce structural distortions of CDs, which lead to increased spin-orbit interaction in them.[2,36]

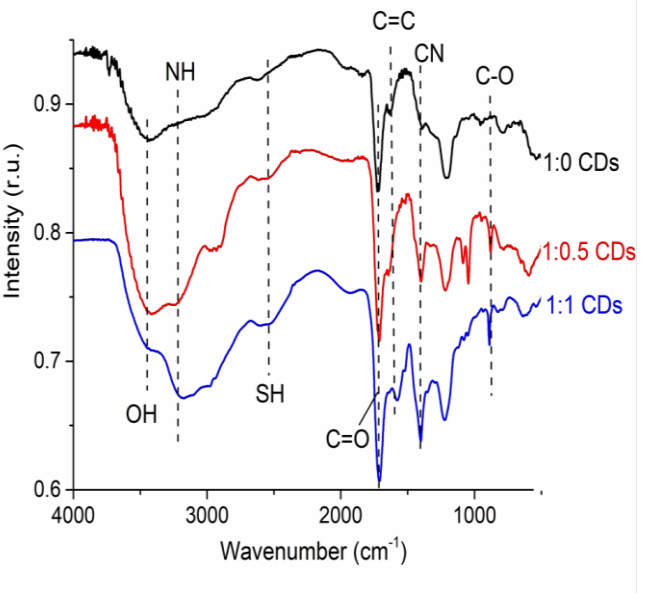

Fig. 2 FTIR spectra of CDs with various CA:L-cysteine ratios.

The XPS spectra of CA-only CDs are presented in Ref. [37] The doping of CDs was confirmed by the XPS data (Fig. 3). In the spectrum of C1s, an intense band at 285 eV can be distinguished, related to C–C and C=C bonds.[38] Bands at ~286.5 eV belong to C–O bonds, and at 288 and 289 eV are the result of the presence of C=O and O–C–O bonds. This is also confirmed by the decomposition of the O1s spectrum, in which two components with maxima of about 531 and 533 eV are distinguishable, responsible for O=C and O–C bonds, respectively.[38] The XPS spectrum of S2p consists of a main band at 163.5 eV, which belongs to S2p$_{3/2}$. This band can be decomposed into three components related to C–SO$_x$ (x=2, 3, 4) bonds. The N1s spectrum of CDs exhibits two peaks at 400.3 and 401.6 eV, which show that nitrogen is present in both pyridine and pyrrole forms.[39]

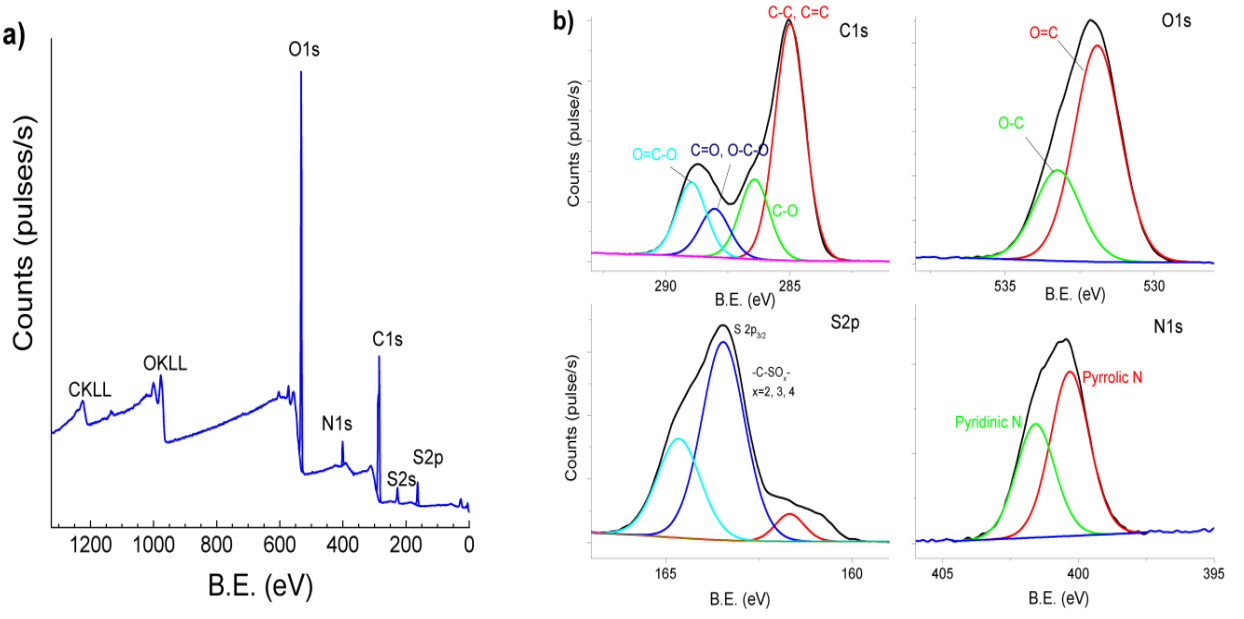

Fig. 3 Survey (a) and a high-resolution (b) XPS spectra of 1:0.5 CDs.

The synthesized CDs have a spherical shape with a diameter from 4±1.5 to 10±1.5 nm (Fig. 4). It was confirmed with the data obtained by the DLS method, where the size of the synthesized CDs varies from 5 to 10 nm. CDs obtained on the basis of pure CA have an average diameter of 2 – 6 nm. The standard deviation in the CDs diameter is ±1.62 nm.

The absorption spectra of the studied CDs in water are shown in the Fig. 5. The absorption spectrum of CDs without heteroatoms in the structure (ratio 1:0) exhibits as a falling curve in the UV range with no pronounced maxima. The absorption spectrum of the doped CDs exhibits a band with a maximum at 348 nm, as well as a shoulder that is about 240 – 250 nm. In order to be able to compare the luminescent properties of CDs in solutions, they were diluted so that their optical density was approximately the same at 350 nm.

In Ref. [7], the dependence of the position of the fluorescence band of CDs and its intensity on the excitation wavelength was studied. It has been demonstrated that the best luminescence can be achieved under the excitation of CDs solutions at λ_{exc}=350 nm. As can be seen from Fig. 5, for 1:0 CDs the maximum of the fluorescence band falls at 445 nm and shifts to 436 nm with an increase in the content of L-cysteine used in synthesis. The highest fluorescence intensity was recorded for solutions of S,N-doped CDs.

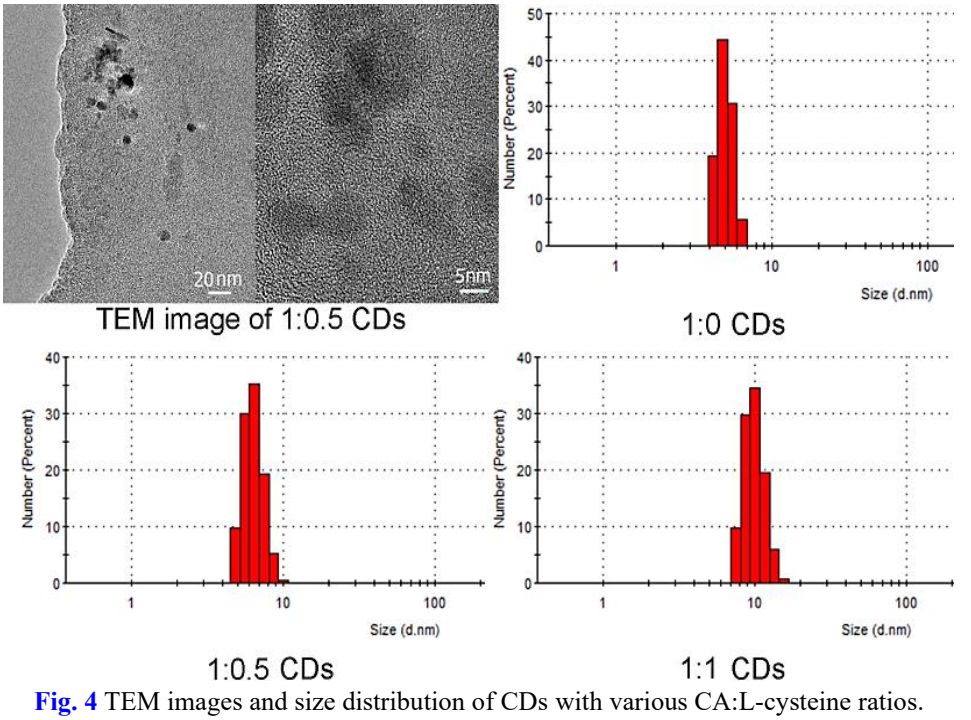

Fig. 4 TEM images and size distribution of CDs with various CA:L-cysteine ratios.

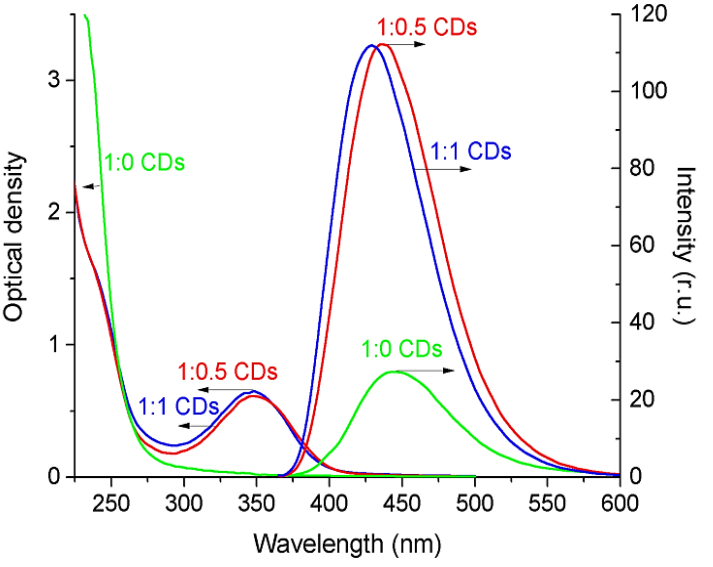

Fig. 5 Absorption and fluorescence (λ_{exc}=350 nm) spectra of CDs solutions with various CA:L-cysteine ratios.

The observed hypsochromic shift of the fluorescence spectra of doped CDs may be due to the fact that at such dots, despite the larger number of formed sp^2-domains of carbon in the core, the degree of their conjugation is low due to additional functionalization, as it was shown by FTIR and XPS data.[40] This leads to the formation of blue-shifted luminescence. In CDs 1:0, the conjugation factor of sp^2-sites is higher, which is expressed in a small bathochromic shift of the fluorescence spectrum.[1,3] This hypothesis is also supported by greater fluorescence intensity in S,N-doped CDs in comparison with the luminescence yield of CDs based on CA-only. A significant decrease in the fluorescence quantum yield of CDs 1:0 is a consequence of an growth of the nonradiative transitions rate due to an increase in the conjugation factor of sp^2-sites in their carbon core.[40]

The absorption spectra of the films of studied CDs are shown on the Fig. 6a. The absorption spectrum of CDs 1:0 exhibits as a decreasing curve in the UV range without pronounced maxima. In the absorption spectrum of doped CDs a band with a maximum at 360 nm, as well as a shoulder at about 240–250 nm was observed. The long-wavelength absorption band is associated with $n\rightarrow\pi^*$ transitions in CDs, while the absorption at 200 nm and the shoulder at 250 nm are associated with $\pi\rightarrow\pi^*$ transitions, respectively.[31] It should be noted that, despite the same volume of solution used for the formation of solid films, the optical density of the band at ~360 nm increases with the growth of the L-cysteine proportion in CDs.

For the CDs films, we also used light with λ_{exc}=350 nm for the excitation of the fluorescence. Measurements showed that 1:0 CDs have low-intensity fluorescence with a band maximum at 430–440 nm (Fig. 6b). Films based on CDs with a ratio of CA:L-cysteine equal to 1:0.5 have the best luminescent ability. A further increase in the L-cysteine part leads to the quenching of fluorescence, as can be seen from the values of φ_{fl} (Table 1).

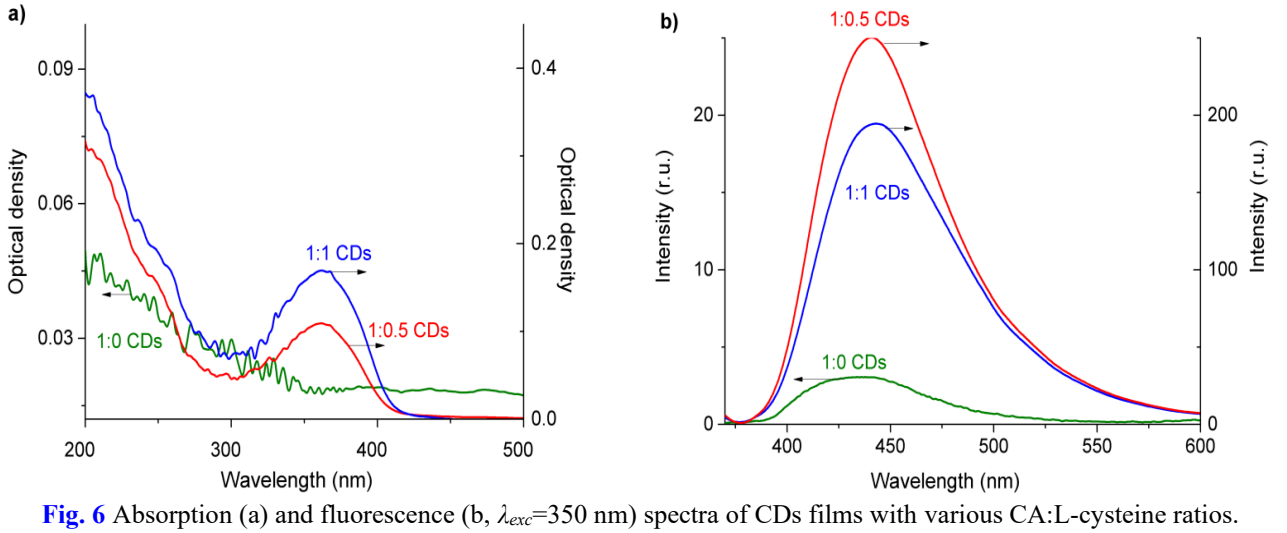

Fig. 6 Absorption (a) and fluorescence (b, λ_{exc}=350 nm) spectra of CDs films with various CA:L-cysteine ratios.

The fluorescence lifetime of the samples depends on the composition of the CDs (Fig. 7, Table 1). The estimated values of φ_{fl} are in the good agreement with the results of Refs. [7,39] for S,N-doped CDs based on CA and L-cysteine. In these works, dots were obtained by the hydrothermal method or with a microwave oven, and the value of φ_{fl} for S,N-doped CDs was about 85–55%.

It can be seen from the obtained data that a correlation is observed between the lifetime (τ_{fl}) and quantum yield (φ_{fl}) of CDs fluorescence. It is known that the high fluorescence quantum yield is associated with the long lifetime of the excited state.[42] The decrease in the lifetime of emission is associated with an increase in the non-radiative channel of decay of the CDs excited state. This leads to a reduction in the number of particles deactivated through the radiative path. The maximum values of τ_{fl} and φ_{fl} were obtained for the ratio of CA and L-cysteine equal to 1:0.5. An increase in the proportion of L-cysteine apparently leads to an increase in the nonradiative decay channel of excited CDs due to some structural transformations.

Table 1. Spectral and luminescent properties* of CDs films with various CA:L-cysteine ratios.

CA:L-cysteine ratio	λ_{max}^{abs} (nm)	λ_{max}^{fl} (nm)	τ_{fl} (ns)	λ_{max}^{LL} (nm)	φ_{fl} (%)
1:0	–	430	1.2±0.2	560	0.40
1:0.5	360	435	5.0±0.2	560	70.8
1:1	360	440	3.8±0.2	560	53.7

*λ_{max}^{abs} – wavelength of the absorption spectrum maximum, λ_{max}^{fl} – wavelength of the fluorescence spectrum maximum, τ_{fl} – fluorescence lifetime, λ_{max}^{LL} – wavelength of the maximum of long-lived luminescence; φ_{fl} – fluorescence quantum yield.

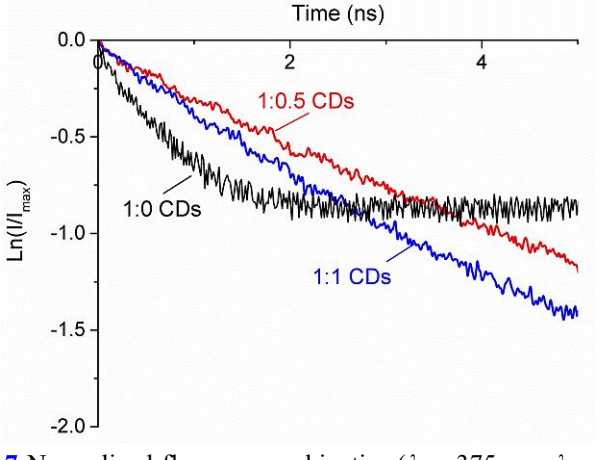

Fig. 7 Normalized fluorescence kinetics (λ_{exc}=375 nm, λ_{reg}=455 nm) of CDs films with various CA:L-cysteine ratios.

During the measurement of the long-lived luminescence for the citric acid-based CDs, a low-intensity luminescence band with a maximum (λ_{max}^{LL}) at 560 nm and shoulder at ~ 400 – 470 nm was observed in the region of 400 – 600 nm (Fig. 8a). For S,N-doped CDs long-lived luminescence was registered in the same region with λ_{max}^{LL}=560 nm. With an increase in the number of sulfur and nitrogen atoms in CDs, an increase in the luminescence intensity was observed.

To confirm the nature of a long-lived emission in doped CDs, the afterglow spectra of 1:0.5 CDs were measured with a change of the film temperature and the pressure in the cryostat (Fig. 8b). It can be seen that the intensity of the long-wavelength luminescence band with λ_{max}=560 nm and its duration increases with decreasing temperature (Fig. 8b). An increase in oxygen concentration above the surface of the sample leads to quenching of the luminescence. From these data it follows that the luminescence band with a maximum at 560 nm can be interpreted as phosphorescence ($T_1 \rightarrow S_0$).[2,43] The appearance of phosphorescence in solid carbon films is quite expected, because in the solid state, the processes of internal conversion and oxygen quenching are partially deactivated, which increases the probability of intersystem crossing (ISC) from the excited singlet state (S_1) to the triplet state (T_1).[2,5,43]

On the contrary, the intensity of the CDs luminescence at 440 nm increases slightly with increasing sample temperature. At the same time, the duration of the luminescence decreases. The addition of oxygen to the volume of the cryostat also leads to quenching of the luminescence (Fig. 8b). The short-wavelength band (λ_{max}= 440 nm) coincides with the fast fluorescence spectrum. The lifetime is close to the phosphorescence lifetime τ_{Ph} (Table 2). The dependence of the intensity and lifetime on temperature and oxygen indicates its triplet nature. The observed luminescence could be attributed to thermally-activated delayed fluorescence (TADF).[36,43] However, the energy splitting between the S_1 and T_1 levels ΔE_{ST}, estimated from the difference in the band maxima, is ~4700 cm^{-1}. With this value of ΔE_{ST}, observation of TADF is unlikely event at room temperature or below.[34,44] It can be assumed that this luminescence is associated with the static annihilation of closely spaced triplet CDs. The number of annihilating pairs will increase with growing of their mobility and growth in the temperature. This will be expressed in the increased intensity of annihilation delayed fluorescence (DF). The lifetime of the annihilation DF is equal to $\tau_{DF}=\frac{1}{2}\tau_{Ph}$. The experimental data don't show this dependence. Non-compliance of this condition may be is due to the fact that high-intensity phosphorescence contributes to the recorded signal at 440 nm, along with annihilation DF. This also explains the resulting trend of the curve of luminescence intensity at 440 nm with temperature, since phosphorescence and annihilation DF have opposite dependences on temperature.

Thus, the long-lived luminescence of solid films of CDs based on CA and L-cysteine has a triplet nature. Phosphorescence is the result of the presence of localized sp^2-carbon domains in CDs. Upon photoexcitation, the singlet–excited (S_1) states of the CDs are populated. The presence of oxygen-containing groups in the structure of 1:0 CDs promote

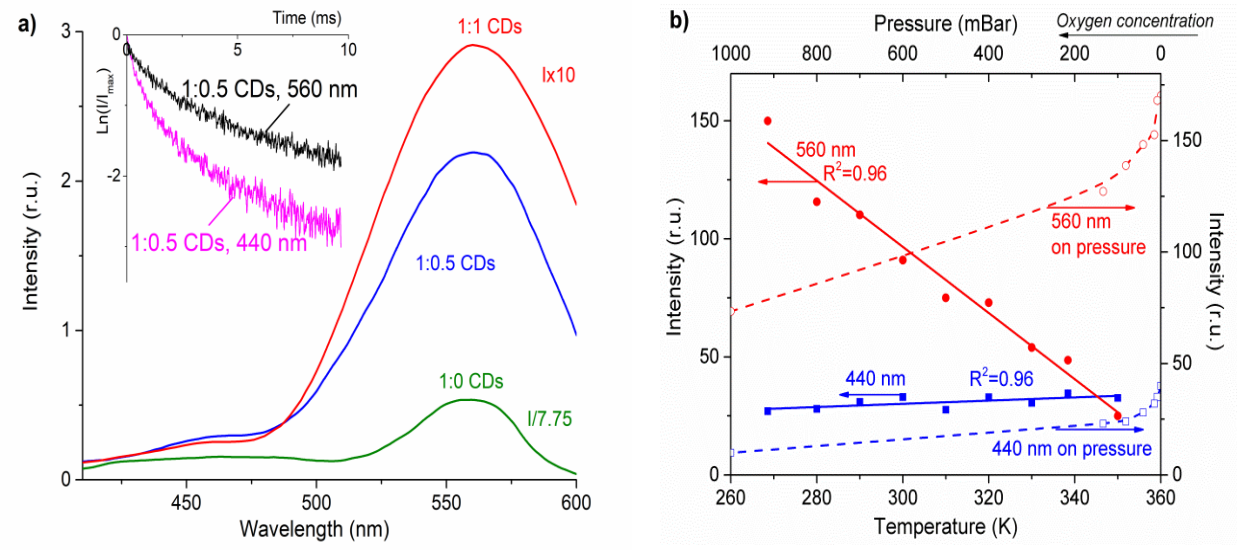

Fig. 8 (a) Long-lived luminescence spectra of CDs films with various CA:L-cysteine ratios (λ_{exc}=350 nm, T=293 K, p=2·10^{-4}mBar). The intensity of the spectrum for 1:0 CDs is increased by 7.75 times, and for 1:1 CDs – is decreased by 10 times. In the inset – long-lived luminescence decay kinetics of 1:0.5 CDs registered at 440 and 560 nm. (b) Dependence of intensity of long-lived luminescence of 1:0.5 CDs at 440 and 560 nm via temperature of the sample and pressure.

the formation of triplet states due to the $S_1 \rightsquigarrow T_n$ interconversion. These groups create deformation modes outside the plane of the carbon domains, which, as known, lead to a decrease in singlet-triplet splitting in CDs.[6,45] The intense manifestation of phosphorescence due to the $T_1 \rightarrow S_0$ transition becomes possible due to the substitution of oxygen-containing groups with S– and N–groups.[45] Apparently, all these processes are reflected in the kinetics of long-lived luminescence, which are described by the bi-exponential law (Table 2).

Table 2. Lifetime of long-lived luminescence (λ_{reg}=440 nm and λ_{reg}=560 nm) of CDs films with various CA:L-cysteine ratios at λ_{exc}=350 nm, T=293 K, p=2·10^{-4} mbar.

CA:L-cysteine ratio	τ_1 (ms)	σ_1 (%)	τ_2 (ms)	σ_2 (%)	τ_{av} (ms)
λ_{reg}=440 nm					
1:0.5	0.4±0.03	29.0	2.7±0.12	71.0	2.0
1:1	0.3±0.03	12.0	2.1±0.12	88.0	1.9
λ_{reg}=560 nm					
1:0.5	0.7±0.03	17.0	3.5±0.12	83.0	3.0
1:1	0.5±0.03	12.0	3.2±0.12	89.0	2.9

One of the way to influence the luminescence ability of molecular systems is the use of plasmon resonance effect of metal nanoparticles.[19-22] Due to the strong local electric field near the plasmon NPs, the properties of the electronically excited states of organic fluorophores change as a result of the electrodipole interaction of excited molecules with plasmons.[24]

We have carried out studies on the effect of plasmon resonance of Ag NPs on the fluorescence ($S_1 \rightarrow S_0$) and phosphorescence ($T_1 \rightarrow S_0$) of CDs of various compositions in films. The specificity of triplet excited states T_1 of molecules lays in their interaction with singlet states S_1 due to the spin-orbit interaction (SOI) between T_1 and S_1. The phosphorescent transition $T_1 \rightarrow S_0$ is only possible due to the borrowing of the intensity of such transition from the allowed $S_1 \rightarrow S_0$ radiative transition. The borrowing factor is proportional to the value of the matrix element of the SOI of T_1 and S_1 states.[21,46] Due to the fact that plasmonic effects manifest themselves in spin-allowed radiative transitions $S_1 \rightarrow S_0$, one can expect the influence of plasmonic NPs on radiative triplet-singlet transitions.

Since S,N-doped CDs with a high luminescence capacity are more promising for practical use, the study of the effect of plasmon resonance of Ag NPs was carried out for 1:0.5 and 1:1 CDs films.

The measurements have shown that the maximum of the absorption band of the SIF exhibits at 440 nm (Fig. 9). On the surface of the SIF, an increase in the optical density (D) of the CDs was observed in both short- and long-wavelength bands. So, for 1:0.5 CDs, the D values were increased by 3.45 times, and for 1:1 CDs – by 1.9 times. At the same time, noticeable shift or deformation of the luminescence bands was not registered on the surface of the silver films.

The enhancement of the optical absorption of fluorophores near the plasmonic NPs is a well-known fact, since large electric fields near the metal nanoparticle caused by confidential plasmonic resonances, leading to a sharp increase in the optical response of the molecule. It was specified by several the authors that such an increase can be associated with both an increase in the excitation rate of dye molecules near the metallic NPs,[22,25] so it is with the modification of the fluorophore oscillator strength and its polarization.[47]

In the presence of SIF, an increase in the intensity of both fast fluorescence and phosphorescence of CDs films is

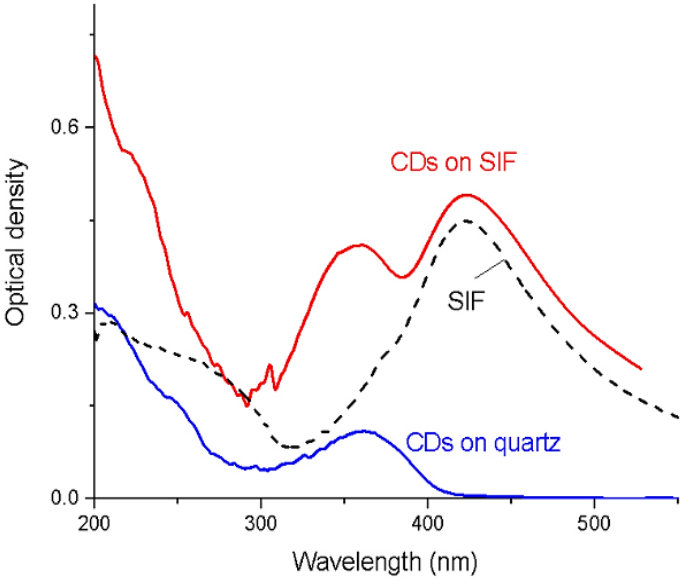

Fig. 9 Absorption spectra of the SIF and 1:0.5 CDs film on the surface of glass and SIF.

observed (Fig. 10, Table 3). The greatest increase in the fluorescence intensity was recorded for 1:1 CDs, where the fluorescence signal was increased by 60%. The lifetime of fluorescence decreases by 28%. For 1:0.5 CDs, the increase in the fluorescence was equal to 30%, and the decrease in the duration of fast fluorescence was equal to 14%. The shortening of the fluorescence lifetime is associated with an increase in the rate of radiative decay of CDs in the near field of silver NPs.[19,22]

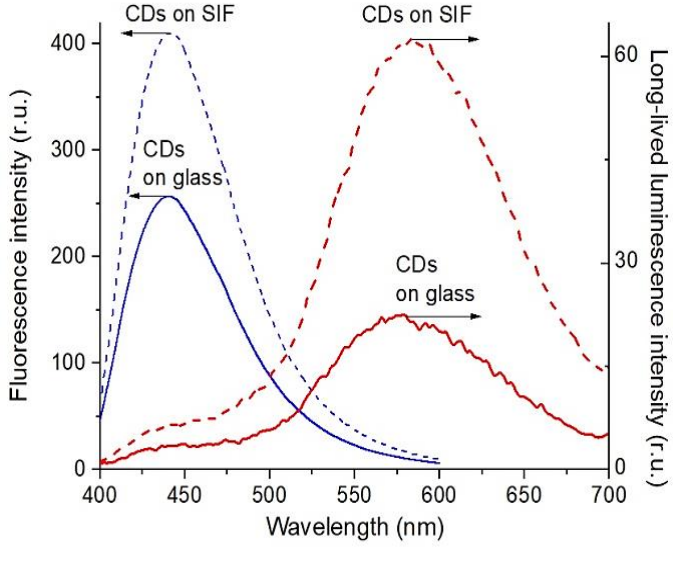

Fig. 10 Spectra of fluorescence (left) and long-lived luminescence (right) of 1:1 CDs films on the glass and on the SIF surfaces, λ_{exc}=350 nm.

The phosphorescence of S,N-doped CDs in the presence of plasmonic NPs increases more than the fluorescence (Fig. 10). As in the case of fluorescence, the highest growth of phosphorescence intensity was registered for 1:1 CDs. The lifetime of long-lived luminescence decreases slightly in this case. This indicates an increase in the rate of radiative decay $T_1 \rightarrow S_0$ of CDs in the presence of Ag NPs.

It is likely that the observed difference in the magnitude of the plasmon effect on the CDs luminescence is associated with a characteristic feature of this phenomenon to influence on processes with a lower quantum efficiency.[19,22] As it were shown (Table 1), φ_{fl}≈71% for 1:0.5 CDs and φ_{fl}≈54% for 1:1 CDs. Thus, it can be expected that the plasmon enhancement of the fluorescence intensity will be of greater for 1:1 CDs.

Table 3. Enhancement coefficients for fluorescence (at λ_{reg}=440 nm) and phosphorescence (at λ_{reg}=560 nm) intensity and lifetimes of CDs with various CA:L-cysteine ratios on the glass and on the SIF surfaces.

CA:L-cysteine ratio	I^{fl}/I_o^{fl}	I^{PH}/I_o^{PH}	$\tau_{SIF}^{fl}/\tau_g^{fl}$	$\tau_{SIF}^{PH}/\tau_g^{PH}$
1:0.5	1.3	2.2	0.86	0.90
1:1	1.6	2.7	0.72	0.88

4. Conclusions

Studies of the structural properties of S- and N-doped CDs have shown that the change in the ratio of precursors does not have a noticeable effect on the size and morphology of carbon dots. The sizes of synthesized CDs vary from 4 to 10 nm. During the study of spectral-luminescent properties of CDs with various compositions, it was found that in L-cysteine-doped CDs, an absorption band with a maximum of 350 nm is additionally manifested in the absorption spectrum, where, as for non-doped CDs it was practically absent. The best emissivity was observed for the films based on CDs with a ratio of CA:L-cysteine equal to 1:0.5. The triplet-excited states are efficiently generated in the synthesized CDs. Their deactivation is possible in two ways – through phosphorescence (λ_{max}=560 nm) and DF (λ_{max}=440 nm). The effect of silver NPs on the absorption and luminescence of CDs films was studied. It was demonstrated for the first time that the presence of Ag NPs leads to the growth in the intensity of long-lived luminescence of CDs. The intensity of fluorescence was increased by 1.6 times, and long-lived luminescence – by 2.7 times. The effect of the CDs luminescence enhancement can be in demand in such applications as photodynamic therapy, bioimaging, anti-counterfeiting coatings and latent imaging, organic light-emitting diodes (OLEDs), sensors, *etc*.

Acknowledgements

This research is funded by the Science Committee of the Ministry of Science and Higher Education of the Republic of Kazakhstan (Grant No. AP09259913).

Conflict of Interest

There is no conflict of interest.

Supporting Information

Not applicable.

References

[1] D. Qu, Z. Sun, The formation mechanism and fluorophores of carbon dots synthesized *via* a bottom-up route, *Materials Chemistry Frontiers*, 2020, **4**, 400-420, doi: 10.1039/c9qm00552h.

[2] B. Wang, S. Lu, The light of carbon dots: from mechanism to applications, *Matter*, 2022, **5**, 110-149, doi: 10.1016/j.matt.2021.10.016.

[3] Y. Xu, C. Wang, G. Ran, D. Chen, Q. Pang, Q. Song, Phosphate-assisted transformation of methylene blue to red-emissive carbon dots with enhanced singlet oxygen generation for photodynamic therapy, *ACS Applied Nano Materials*, 2021, **4**, 4820-4828, doi: 10.1021/acsanm.1c00406.

[4] J. Yue, L. Li, C. Jiang, Q. Mei, W.-F. Dong, R. Yan, Riboflavin-based carbon dots with high singlet oxygen generation for photodynamic therapy, *Journal of Materials Chemistry B*, 2021, **9**, 7972-7978, doi: 10.1039/d1tb01291f.

[5] J. Zhu, X. Bai, X. Chen, H. Shao, Y. Zhai, G. Pan, H. Zhang, E. V. Ushakova, Y. Zhang, H. Song, A. L. Rogach, Spectrally tunable solid state fluorescence and room-temperature phosphorescence of carbon dots synthesized via seeded growth method, *Advanced Optical Materials*, 2019, **7**, 1801599, doi: 10.1002/adom.201801599.

[6] M. Park, H. S. Kim, H. Yoon, J. Kim, S. Lee, S. Yoo, S. Jeon, Graphene quantum dots: controllable singlet-triplet energy splitting of graphene quantum dots through oxidation: from phosphorescence to TADF (adv. mater. 31/2020), *Advanced Materials*, 2020, **32**, 2000936, doi: 10.1002/adma.202070233.

[7] N. Ibrayev, R. Dzhanabekova, E. Seliverstova, G. Amanzholova, Optical properties of N- and S-doped carbon dots based on citric acid and L-cysteine, *Fullerenes, Nanotubes and Carbon Nanostructures*, 2022, **30**, 22-26, doi: 10.1080/1536383x.2021.1999933.

[8] H. Kang, J. Zheng, X. Liu, Y. Yang, Phosphorescent carbon dots: Microstructure design, synthesis and applications, *New Carbon Materials*, 2021, **36**, 649-664, doi: 10.1016/S1872-5805(21)60083-5.

[9] A. Kim, J. K. Dash, P. Kumar, R. Patel, Carbon-based quantum dots for photovoltaic devices: a review, *ACS Applied Electronic Materials*, 2022, **4**, 27-58, doi: 10.1021/acsaelm.1c00783.

[10] A. Sciortino, N. Mauro, G. Buscarino, L. Sciortino, R. Popescu, R. Schneider, G. Giammona, D. Gerthsen, M. Cannas, F. Messina, β-C_3N_4 nanocrystals: carbon dots with extraordinary morphological, structural, and optical homogeneity, *Chemistry of Materials*, 2018, **30**, 1695-1700, doi: 10.1021/acs.chemmater.7b05178.

[11] K. G. Nguyen, I.-A. Baragau, R. Gromicova, A. Nicolaev, S. A. J. Thomson, A. Rennie, N. P. Power, M. T. Sajjad, S. Kellici, Investigating the effect of N-doping on carbon quantum dots structure, optical properties and metal ion screening, *Scientific Reports*, 2022, **12**, 13806, doi: 10.1038/s41598-022-16893-x.

[12] E. Seliverstova, N. Ibrayev, E. Menshova, E. Alikhaidarova, Laser modification of structure and optical properties of N-doped graphene oxide, *Materials Research Express*, 2021, **8**, 115601, doi: 10.1088/2053-1591/ac31fc.

[13] Z. Qian, X. Shan, L. Chai, J. Ma, J. Chen, H. Feng, Si-doped carbon quantum dots: a facile and general preparation strategy, bioimaging application, and multifunctional sensor, *ACS Applied Materials & Interfaces*, 2014, **6**, 6797-6805, doi: 10.1021/am500403n.

[14] K. Luo, Y. Wen, X. Kang, Halogen-doped carbon dots: synthesis, application, and prospects, *Molecules*, 2022, **27**, 4620, doi: 10.3390/molecules27144620.

[15] K. Yuan, R. Qin, J. Yu, X. Li, L. Li, X. Yang, X. Yu, Z. Lu, X. Zhang, H. Liu, Effects of localized surface plasmon resonance of Ag nanoparticles on luminescence of carbon dots with blue, green and yellow emission, *Applied Surface Science*, 2020, **502**, 144277, doi: 10.1016/j.apsusc.2019.144277.

[16] B. Bagra, W. Zhang, Z. Zeng, T. Mabe, J. Wei, Plasmon-enhanced fluorescence of carbon nanodots in gold nanoslit cavities, *Langmuir*, 2019, **35**, 8903-8909, doi: 10.1021/acs.langmuir.9b00448.

[17] Y. Kamura, K. Imura, Photoluminescence from carbon dot-gold nanoparticle composites enhanced by photonic and plasmonic double-resonant effects, *ACS Omega*, 2020, **5**, 29068-29072, doi: 10.1021/acsomega.0c03588.

[18] A. Sciortino, A. Panniello, G. Minervini, N. Mauro, G. Giammona, G. Buscarino, M. Cannas, M. Striccoli, F. Messina, Enhancing carbon dots fluorescence via plasmonic resonance energy transfer, *Materials Research Bulletin*, 2022, **149**, 111746, doi: 10.1016/j.materresbull.2022.111746.

[19] E. Seliverstova, N. Ibrayev, G. Omarova, A. Ishchenko, M. Kucherenko, Competitive influence of the plasmon effect and energy transfer between chromophores and Ag nanoparticles on the fluorescent properties of indopolycarbocyanine dyes, *Journal of Luminescence*, 2021, **235**, 118000, doi: 10.1016/j.jlumin.2021.118000.

[20] N. Ibrayev, E. Seliverstova, N. Zhumabay, D. Temirbayeva, Plasmon effect in the donor-acceptor pairs of dyes with various efficiency of FRET, *Journal of Luminescence*, 2019, **214**, 116594, doi: 10.1016/j.jlumin.2019.116594.

[21] D. Temirbayeva, N. Ibrayev, M. Kucherenko, Distance dependence of plasmon-enhanced fluorescence and delayed luminescence of molecular planar nanostructures, *Journal of Luminescence*, 2022, **243**, 118642, doi: 10.1016/j.jlumin.2021.118642.

[22] C. D. Geddes, J. R. Lakowicz, Metal-Enhanced Fluorescence, *Journal of Fluorescence*, 2022, **12**, 121-129, doi: 10.1023/A:1016875709579.

[23] H. Abdolmohammad-Zadeh, Z. Azari, E. Pourbasheer, Fluorescence resonance energy transfer between carbon quantum dots and silver nanoparticles: application to mercuric ion sensing, *Spectrochimica Acta Part A: Molecular and Biomolecular Spectroscopy*, 2021, **245**, 118924, doi: 10.1016/j.saa.2020.118924.

[24] N. A. Ahmad Nazri, N. H. Azeman, M. H. Abu Bakar, N. N. Mobarak, Y. Luo, N. Arsad, T. H. T. A. Aziz, A. R. M. Zain, A. A. A. Bakar, Localized surface plasmon resonance decorated with carbon quantum dots and triangular Ag nanoparticles for

chlorophyll detection, *Nanomaterials*, 2021, **12**, 35, doi: 10.3390/nano12010035.
[25] M. Amjadi, R. Shokri, T. Hallaj, Interaction of glucose-derived carbon quantum dots with silver and gold nanoparticles and its application for the fluorescence detection of 6-thioguanine, *Luminescence*, 2017, **32**, 292-297, doi: 10.1002/bio.3177.
[26] R. Knoblauch, B. Bui, A. Raza, C. D. Geddes, Heavy carbon nanodots: a new phosphorescent carbon nanostructure, *Physical Chemistry Chemical Physics*, 2018, **20**, 15518-15527, doi: 10.1039/c8cp02675k.
[27] C. Fowley, N. Nomikou, A. P. McHale, B. McCaughan, J. F. Callan, Extending the tissue penetration capability of conventional photosensitisers: a carbon quantum dot-protoporphyrin IX conjugate for use in two-photon excited photodynamic therapy, *Chemical Communications*, 2013, **49**, 8934, doi: 10.1039/c3cc45181j.
[28] M. Kováčová, Z. M. Marković, P. Humpolíček, M. Mičušík, H. Švajdlenková, A. Kleinová, M. Danko, P. Kubát, J. Vajďák, Z. Capáková, M. Lehocký, L. Münster, B. M. Todorović Marković, Z. Špitalský, Carbon quantum dots modified polyurethane nanocomposite as effective photocatalytic and antibacterial agents, *ACS Biomaterials Science & Engineering*, 2018, **4**, 3983-3993, doi: 10.1021/acsbiomaterials.8b00582.
[29] Y. Zhou, H. Sun, F. Wang, J. Ren, X. Qu, How functional groups influence the ROS generation and cytotoxicity of graphene quantum dots, *Chemical Communications*, 2017, **53**, 10588-10591, doi: 10.1039/c7cc04831a.
[30] B. Minaev, The spin of dioxygen as the main factor in pulmonology and respiratory care, *Archives of Pulmonology and Respiratory Care*, 2022, **8**, 28-33, doi: 10.17352/aprc.000081.
[31] L. Shi, J. H. Yang, H. B. Zeng, Y. M. Chen, S. C. Yang, C. Wu, H. Zeng, O. Yoshihito, Q. Zhang, Carbon dots with high fluorescence quantum yield: the fluorescence originates from organic fluorophores, *Nanoscale*, 2016, **8**, 14374-14378, doi: 10.1039/c6nr00451b.
[32] L. Novotny, B. Hecht, Principles of Nano-Optics, Cambridge: Cambridge University Press, 2006, doi: 10.1017/cbo9780511813535.
[33] W. Becker, The bh TCSPC Handbook, 10th Edition, Berlin: Becker&Hickl, 2023, www.becker-hickl.com.
[34] C. A. Parker, Photoluminescence of Solutions, Amsterdam-London-New York: Elsevier publishing Co., 1968.
[35] R. R. Anjana, J. S. Anjali Devi, M. Jayasree, R. S. Aparna, B. Aswathy, G. L. Praveen, G. M. Lekha, G. Sony, S,N-doped carbon dots as a fluorescent probe for bilirubin, *Microchimica Acta*, 2017, **185**, 1-11, doi: 10.1007/s00604-017-2574-8.
[36] J. Liu, H. Zhang, N. Wang, Y. Yu, Y. Cui, J. Li, J. Yu, Template-modulated afterglow of carbon dots in zeolites: room-temperature phosphorescence and thermally activated delayed fluorescence, *ACS Materials Letters*, 2019, **1**, 58-63, doi: 10.1021/acsmaterialslett.9b00073.
[37] N. Ibrayev, E. Seliverstova, G. Amanzholova, Activation of molecular oxygen by triplet states of S,N-doped carbon dots, *Chemical Physics Letters*, 2023, **833**, 140947, doi: 10.1016/j.cplett.2023.140947.
[38] Q. Xu, P. Pu, J. Zhao, C. Dong, C. Gao, Y. Chen, J. Chen, Y. Liu, H. Zhou, Preparation of highly photoluminescent sulfur-doped carbon dots for Fe(iii) detection, *Journal of Materials Chemistry A*, 2015, **3**, 542-546, doi: 10.1039/c4ta05483k.
[39] Y. Dong, H. Pang, H. B. Yang, C. Guo, J. Shao, Y. Chi, C. M. Li, T. Yu, Carbon-based dots co-doped with nitrogen and sulfur for high quantum yield and excitation-independent emission, *Angewandte Chemie International Edition*, 2013, **52**, 7800-7804, doi: 10.1002/anie.201301114.
[40] N. V. Tepliakov, E. V. Kundelev, P. D. Khavlyuk, Y. Xiong, M. Y. Leonov, W. Zhu, A. V. Baranov, A. V. Fedorov, A. L. Rogach, I. D. Rukhlenko, sp^2-sp^3-hybridized atomic domains determine optical features of carbon dots, *ACS Nano*, 2019, **13**, 10737-10744, doi: 10.1021/acsnano.9b05444.
[41] F. Gao, S. Ma, J. Li, K. Dai, X. Xiao, D. Zhao, W. Gong, Rational design of high-quality citric acid-derived carbon dots by selecting efficient chemical structure motifs, *Carbon*, 2017, **112**, 131-141, doi: 10.1016/j.carbon.2016.10.089.
[42] J. R. Lakowicz, Y. Fu, Modification of single molecule fluorescence near metallic nanostructures, *Laser & Photonics Reviews*, 2009, **3**, 221-232, doi: 10.1002/lpor.200810035.
[43] K. Jiang, Y. Wang, Z. Li, H. Lin, Afterglow of carbon dots: mechanism, strategy and applications, *Materials Chemistry Frontiers*, 2020, **4**, 386-399, doi: 10.1039/c9qm00578a.
[44] T. Chen, L. Zheng, J. Yuan, Z. An, R. Chen, Y. Tao, H. Li, X. Xie, W. Huang, Understanding the control of singlet-triplet splitting for organic exciton manipulating: a combined theoretical and experimental approach, *Scientific Reports*, 2015, **5**, 10923, doi: 10.1038/srep10923.
[45] D. Dou, J. Duan, Y. Zhao, B. He, Q. Tang, Cubic carbon quantum dots for light-harvesters in mesoscopic solar cells, *Electrochimica Acta*, 2018, **275**, 275-280, doi: 10.1016/j.electacta.2018.04.124.
[46] S.P. McGlynn, T. Azumi, M. Kinoshita, Molecular spectroscopy of the triplet state. New Jersey: Prentice-Hall, 1969.
[47] S. M. Morton, D. W. Silverstein, L. Jensen, Theoretical studies of plasmonics using electronic structure methods, *Chemical Reviews*, 2011, **111**, 3962-3994, doi: 10.1021/cr100265f.